J. Fluid Mech. (2001), *vol.* 429, *pp.* 217–238. Printed in the United Kingdom

Wake formation around islands in oscillatory laminar shallow-water flows. Part 1. Experimental investigation

By PETER M. LLOYD[1]†, PETER K. STANSBY[1] AND DAOYI CHEN[2]

[1]Department of Civil and Construction Engineering, UMIST, Manchester M60 1QD, UK

[2]School of Engineering, University of Manchester, Manchester M13 9PL, UK

(Received 3 July 1998 and in revised form 4 August 2000)

An experimental investigation of oscillatory shallow-water flow around islands has been undertaken to determine the dependence of wake formation on Keulegan–Carpenter number, $KC = U_o T/D$, and stability parameter, $S = c_f D/h$, where U_o is amplitude of velocity oscillation, T is oscillation period, D is a representative island diameter, c_f is friction coefficient and h is water depth. Two geometries are investigated: a vertical cylinder and a conical island with a small side slope of 8°. Existing experimental results for current flow around the same geometries have shown the influence of the stability parameter. Predominantly laminar flows are investigated and the flows are subcritical.

Four modes of wake formation have been identified for both geometries: one with symmetric attached counter-rotating vortices only forming in each half-cycle, one with vortex pairs forming symmetrically in addition in each half-cycle, one with vortex pairs forming with some asymmetry and one with complex vortex shedding. The last results from one of the attached vortices crossing to the opposite side of the body during flow reversal; in the other cases the attached vortices are convected back on the same sides. For convenience these formations are called: symmetric without pairing, symmetric with pairing, sinuous with pairing and vortex shedding. They are shown on KC/S planes for both geometries. Numerical modelling of the flows for the conical island, based on the three-dimensional shallow-water equations with the hydrostatic pressure assumption, is undertaken in Part 2 (Stansby & Lloyd 2001).

1. Introduction

Recirculation zones in shallow-water tidal flows are generated by headlands, islands and other topographies and have a dominant effect on mixing processes relevant to pollution dispersion and sediment transport. Large-scale recirculation zones have been shown in satellite images and aerial photographs, e.g. Wolanski, Imberger & Heron (1984), Pattiaratchi, James & Collins (1986) and Ingram & Chu (1987), and numerous numerical studies have been made based on the shallow-water equations. However, the complexities of these flows are not well understood and, quite apart from the assumptions inherent in the shallow-water equations, many (probably all) numerical simulations are affected by numerical diffusion and wave damping.

† Present address: Tessella Support Services plc, Robert Gordon House, Cavendish Avenue, Birchwood Park, Warrington WA3 6FT, UK.

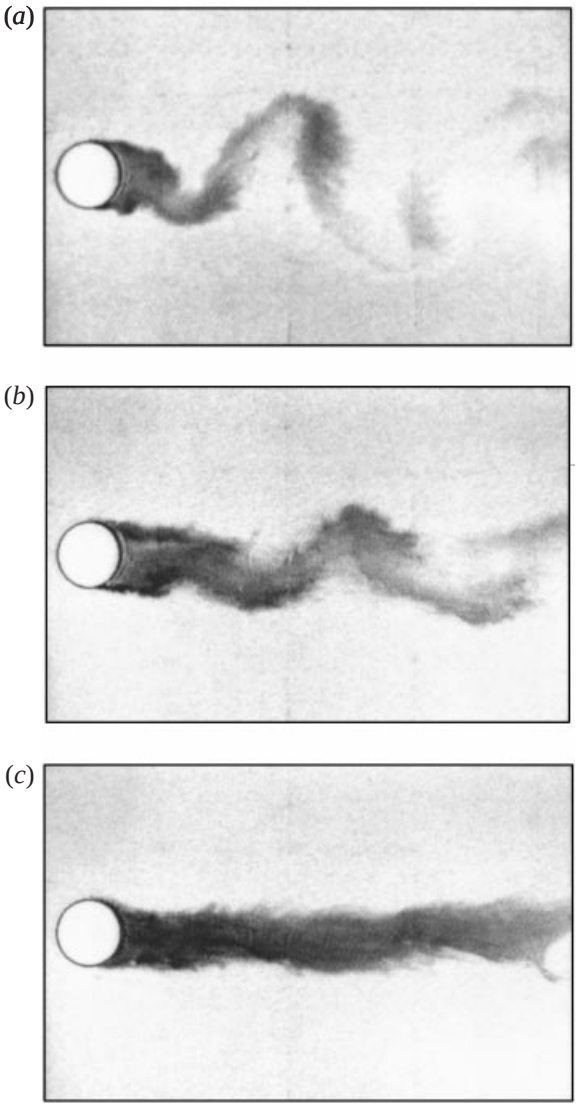

FIGURE 1. Wake structures generated in a steady free stream. (*a*) $S = 0.060$, (*b*) $S = 0.213$, (*c*) $S = 0.371$.

Flows around islands generate recirculation zones typical of shallow-water flows and we choose simple circular cross-sections for fundamental investigation. Experiments with steady current flow for vertical circular cylinders (Chen & Jirka 1995) and conical islands of small side slope (Lloyd & Stansby 1997) have shown how wake formation is controlled by the stability parameter, $S = c_f D/h$, where c_f is friction coefficient, h is water depth and D is the diameter at mid-depth in the conical island case. For $S < 0.2$, vortices were shed periodically from the island in the manner of a Kármán vortex street; for $S > 0.5$ two steady counter-rotating recirculation zones were generated (a steady-bubble wake) and for $0.2 < S < 0.5$ an unsteady-bubble wake was formed. Dye visualization of these wake formations is shown in figure 1. Linear stability analysis of the depth-averaged shallow-water equations with bed friction using a time-averaged transverse near-wake velocity profile as input has shown that vortex

shedding corresponds to an absolute instability, where temporal/spatial evolution of a disturbance occurs, and a steady bubble corresponds to a convective instability, where only spatial evolution occurs (Chen & Jirka 1997). This analysis was related to the vertical cylinder experiments and, although the boundary values for S for different wake formations differ by a factor of about two, the vortex-shedding frequency was predicted well. This analysis also draws attention to the similarity between increasing stability parameter in shallow-water flow and decreasing Reynolds number in unbounded cylinder wakes, both causing a wake to become more stable.

Unbounded cylinder wakes in oscillatory flows have also received much attention. Experiments have shown that the complexity of vortex shedding with vortex pairing increases as the Keulegan–Carpenter number, $KC = U_o T/D$, increases, where U_o is amplitude of velocity oscillation and T is oscillation period, e.g. Bearman *et al.* (1981), Williamson (1985), Obasaju, Bearman & Graham (1988). For $KC < 7$ a pair of attached vortices is generated in each half-cycle and is convected back around the cylinder in the following half-cycle forming vortex pairs. This process is quite symmetric for $KC < 4$. For $KC > 7$ vortices are shed: for $7 < KC < 15$ one vortex is shed per half-cycle, for $15 < KC < 24$ two vortices are shed, and so on. For $KC < 2$ numerical simulations for laminar flow (Smith & Stansby 1991) have shown that the flow is predominantly attached, with the pair of attached vortices generated in each half-cycle combining with newly generated vorticity in following half-cycles to form a repetitive oscillatory three-pair system. For $KC < 1$ however only a single pair of attached vortices is visible. These general observations appear not to depend significantly on a Stokes parameter, $\beta = Re/KC$, provided it is high enough ($\beta > 200$ say). Here $Re = U_o D/\nu$, where ν is kinematic viscosity. Related vortex-shedding phenomena may be expected in shallow-water flows around islands for small values of the stability parameter, corresponding to high Stokes parameters for unbounded cylinder wakes. It is worth noting here that, while unbounded cylinder flows of practical interest (mainly associated with wave forces on offshore structures) are at very high Reynolds numbers (or Stokes parameter) relating to low stability, in practice shallow-water flows (in tidal situations) often have high values of stability parameter.

In this paper results of a detailed experimental investigation of oscillatory shallow-water flows around islands of circular cross-section are presented, the islands having either vertical sides or sides of small slope (8°) to correspond to previous investigations in a current. The wake structure is defined by the following parameters:

$$T, \quad U_o, \quad \tau_o, \quad \rho, \quad \mu, \quad h, \quad g, \quad D,$$

where τ_o is maximum bed shear stress, ρ is water density, μ is viscosity, g is gravitational acceleration, U_o is here the amplitude of velocity oscillation near the surface (which is outside the boundary layer in these flows) and other parameters have already been defined. Dimensional analysis shows that the following non-dimensional groups may identify wake structure:

$$c_f = \frac{\tau_o}{\frac{1}{2}\rho U_o^2}, \quad KC = \frac{U_o T}{D}, \quad Re_a = \frac{\rho U_o a}{\mu}, \quad \frac{D}{h}, \quad Fr = \frac{U_o}{\sqrt{gh}},$$

where the amplitude of fluid motion $a = U_o T/2\pi$. In these experiments the ambient maximum Froude number, Fr, is always below 0.2 (the value based on the depth-averaged velocity would of course be rather lower). Although locally it may be higher it will be shown to be always be subcritical. For unbounded wakes, wake structure depends on KC and Re_a or Re and, for shallow-water wakes in a current of

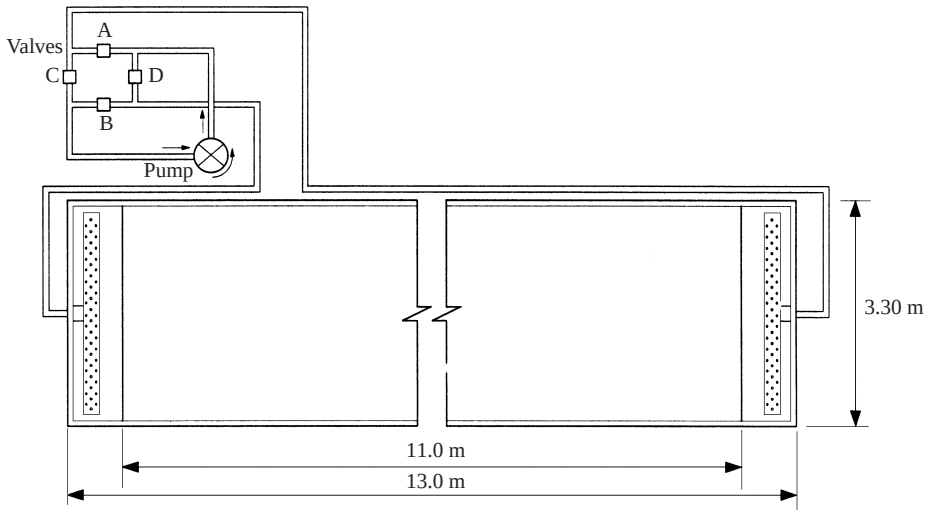

FIGURE 2. A sketch of the shallow-water tidal flume. The valves A, B, C, and D control the direction of the flow.

velocity U (assuming low subcritical Froude number), on c_f, D/h and $Re_h = \rho U h/\mu$ where c_f and D/h may be combined as a stability parameter $S = c_f D/h$ and Re_h is of secondary importance. The formation of the stability parameter is based on the original work of Chu, Wu & Khayat (1991) who showed that the stability of a parallel velocity profile $U(y)$, where y is the cross-stream dimension, is dependent on $(c_f/2h)U/(\partial U/\partial y)$, based on values at maximum $\partial U/\partial y$. For the case of an island of diameter D, $\partial U/\partial y$ is assumed to be proportional to U/D giving a stability parameter $c_f D/h$. Grubišić, Smith & Schär (1995) independently used this parameter in relation to atmospheric flows calling it the non-dimensional bottom friction number describing the ratio of friction to inertia forces. In the case of oscillatory flow such analyses are not appropriate except (possibly) in the quasi-steady case of $KC \to \infty$. However, in view of the success of S in defining wakes in a current, wake formation in oscillatory flow in this study will be assumed initially to be dependent on KC and S with D/h a secondary effect. To avoid the additional complexities associated with turbulence, results for predominantly laminar flow are presented here. Dye visualization and (surface) particle tracking velocimetry (PVT) are used to show the time-dependent wake structures.

2. Experimental set-up

2.1. *The flume and islands*

Experiments were conducted in a 11.0 m × 3.3 m shallow-water tidal flume, illustrated schematically in figure 2. The bed and sidewalls of the flume are constructed from marine plywood, painted to give a smooth finish. Oscillatory current flows with a nearly sinusoidal velocity profile are considered here, generated by a uni-directional variable speed pump and an arrangement of four valves. We can see in figure 2 that with valves A and B closed and C and D open the flow is from left to right. Changing the state of the valves reverses the flow direction. Current velocities and tidal periods were controlled by supplying a sinusoidal voltage input to the pump controller using a PC housed D/A card. An array of aluminium flow straighteners helped to produce

a near-uniform transverse velocity profile with a maximum variation from the mean of approximately $\pm 5\%$.

Two island geometries have been used in this study: a circular cylinder and a conical island. The circular cylinder had a diameter of 0.60 m and a height of 0.08 m. The conical island had a base diameter of 0.75 m and a side slope angle of 8.0° to the horizontal. Both were painted to give a smooth surface finish similar to the flume bed.

2.2. *Particle tracking velocimetry (PTV)*

Surface velocity vector maps have been produced using the digital, particle tracking velocimetry (PTV) method described in Lloyd, Stansby & Ball (1995). Several hundred 8 mm diameter polypropylene beads were released onto the water surface during a run to act as tracer particles, floating at the free surface (almost submerged). The movement of the particles was filmed from above with a ceiling-mounted CCD camera and recorded on video tape. The camera and lens arrangement used here provided a coverage of 2.6 m × 2.6 m. The recordings were replayed through a PC controlled Quintek Mosaiq frame grabber enabling selected frames of film to be digitized. The resolution of the images was 512 × 512 pixels with 256 grey levels. Pairs of digital images were then used as input to a computer program that automatically corrects for image distortion, distinguishes the seeding particles from the background, tracks their movement and calculates their velocity. Individual particles are tracked, which leaves velocity vectors in an unstructured distribution across the image plane and an accurate interpolation procedure was applied to reorganize the spatially scattered data onto a regular grid.

The accuracy of the PTV velocity measurements has previously been assessed by comparison with simultaneous laser Doppler anemometer measurements in the wake of a conical island of 22.2° side slope in a steady free stream (Lloyd *et al.* 1995). Velocities in the wake were unsteady with vigorous vortex shedding a prominent feature. Although the PTV technique did not pick up the small-scale high-frequency velocity components, it did provide a quantitative visualization of the large-scale structures present in the flow, with the average PTV velocity error measured at less than 10%.

2.3. *Flow visualization*

Flow visualization studies have been made using methylene blue dye injected at the side of an island in the transverse shear layers which generate vortex motions in the near wake. As with the PTV studies, the flows were filmed from above, recorded on to video tape and then analysed using the frame grabber. The digitized images were enhanced using a 'contrast stretching' technique, whereby a background image, taken before any dye was injected into the flow, was subtracted from the image of interest. Differences in grey level between the background image and the image to be enhanced (indicating patches of dye) were exaggerated to highlight the dark regions of dye from the light coloured flume background.

2.4. *Test conditions*

Ambient velocity was measured well away from the island with a single-channel Minilab ultrasonic current meter. A typical velocity history is shown in figure 3 which may be approximated as $U = U_o \sin \omega t$, where $\omega = 2\pi/T$ is angular frequency. The small higher frequency components are due to wave oscillations in the flume, which could not be avoided and are present with or without a model in the flume. Sarpkaya

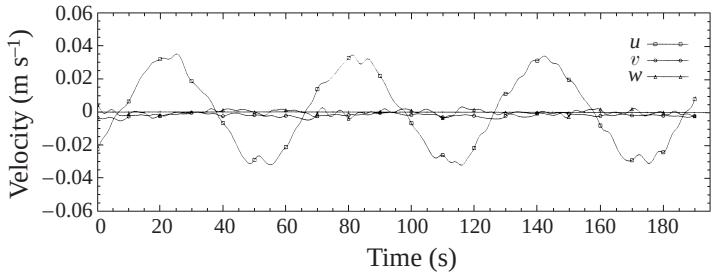

FIGURE 3. Sample velocity record measured using the Nortek ADV. $U_o = 0.035\,\mathrm{m\,s^{-1}}$, $T = 60\,\mathrm{s}$ (case CI02 in table 2). A 21-point digital filter has been used to remove instrument noise (Hamming 1989).

(1993) indicates on the basis of dye visualization that an unbounded smooth-wall oscillatory boundary layer flow will be laminar provided that the oscillatory Reynolds number Re_a is less than approximately 10^5. For the circular cylinder investigation the ambient flow conditions for all but four of the 20 cases investigated cases fall into the range $Re_a < 10^5$, while $Re_a < 1.9 \times 10^5$ for all cases. Measurements of bed shear stress are however predicted well by Stokes' formula for friction coefficient, $c_f = \tau_o/(\frac{1}{2}\rho U_o^2)$, given by $c_f = 2/\sqrt{Re_a}$ up to at least $Re_a = 2 \times 10^5$, as reviewed by Sarpkaya (1993). The tests with Re_a larger than 10^5 give high values of KC of up to 21. The boundary layer thickness is defined by $\frac{3}{4}\pi(2av/U_o)^{1/2}$ (Batchelor 1967) and in these experiments is smaller than the water depth.

For the 17 conical island flows investigated the maximum value of Re_a is 1.07×10^5 and 70% of the runs considered have $Re_a < 0.6 \times 10^5$. It should however be mentioned that for both the cylinder and conical island tests the acceleration of the flow around the body sides might cause some local transitional behaviour during a tidal oscillation.

For a rough surface the transition to turbulent flow will begin at lower values of Re_a than for a smooth bed. According to French (1994) a planed wooden flume has a Nikuradse's equivalent sand grain roughness values k_s of 6×10^{-4}. Jensen *et al.* (1989) define a roughness parameter as a/k_s and a roughness Reynolds number $k_s^+ = k_s U_o^*/\nu$ where U_o^* is the maximum value of the friction velocity, $(\tau_o/\rho)^{1/2}$, during the oscillation period. Using figure 2 of Jensen, Sumer & Fredsøe we find k_s^+ to be less than 4 for all the flows studied here. Jensen *et al.* consider the wall to be smooth for $k_s^+ < 6$.

Assuming a smooth wall and laminar flow the bottom friction coefficient is thus given by $c_f = 2/\sqrt{Re_a}$. The velocity, U_o, defining Re_a is measured at a level of 0.67 of the depth above the bed, which is always above the boundary-layer thickness. The stability parameter $S = c_f D/h$ is thus defined.

3. Results

3.1. *Wake formation for the circular cylinder*

Wake stability in an oscillatory flow is less meaningful than in steady incident flow. In steady flows a wake is classified as stable when vortex shedding does not occur: the counter-rotating vortices (eddies) in the wake remain attached to the cylinder (referred to as steady-bubble flow). In an oscillatory flow the free stream itself is unsteady and vortex pairing or shedding may occur during flow reversal as a result of vortices convecting back past the cylinder. In this study we have classified island

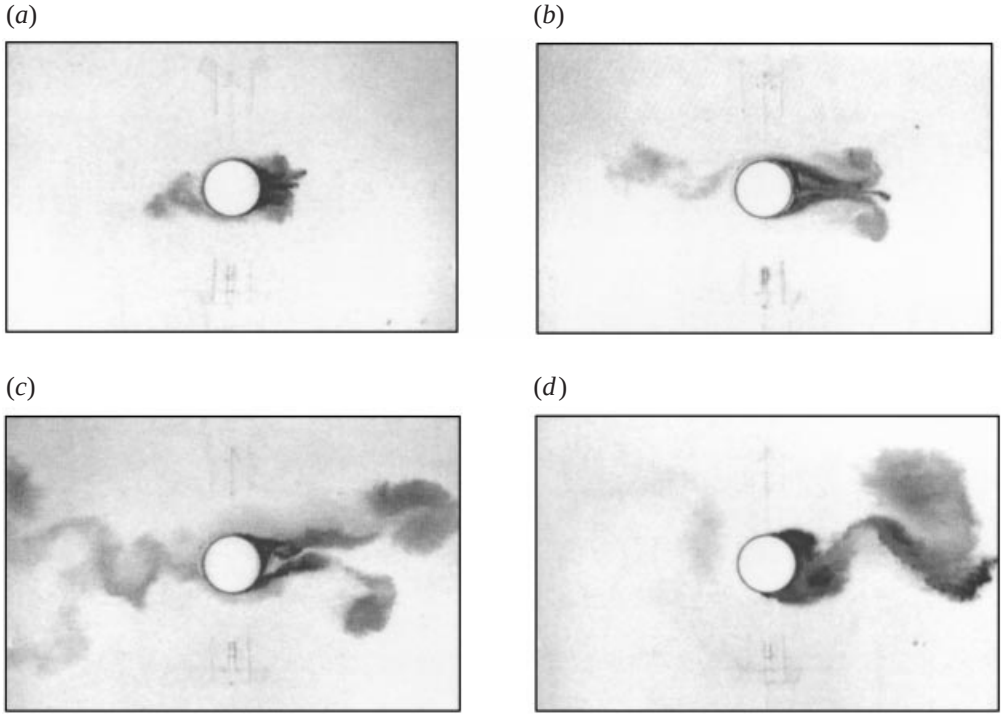

FIGURE 4. Oscillatory shallow-water wakes at time $t = T/4$ (flow moving left to right at maximum velocity) visualized using methylene blue dye. (*a*) symmetric-without-pairing (CC01, $KC = 4.4$, $S = 0.165$); (*b*) symmetric-with-pairing (CC13, $KC = 9.0$, $S = 0.244$); (*c*) sinuous-with-pairing (CC10, $KC = 20.0$, $S = 0.081$); (*d*) vortex-shedding (CC05, $KC = 21.0$, $S = 0.047$).

wakes into four categories: (*i*) *symmetric without vortex pairing,* (*ii*) *symmetric with pairing,* (*iii*) *sinuous with pairing* and (*iv*) *vortex shedding*. Examples of the different wake types are shown in the digitized dye visualization images in figure 4, where each image is produced at time $t = T/4$. For type (*i*) in figure 4(*a*), the most 'stable' of the categories, only attached counter-rotating vortices are formed during a half-cycle. For type (*ii*) in figure 4(*b*), symmetric vortex pairs are formed in a half-cycle as well as the attached counter-rotating vortices. Type (*iii*), in figure 4(*c*), is similar to (*ii*) but has an asymmetric 'sinuous' form. Type (*iv*), in figure 4(*d*), is characterized by vortex shedding.

The dependence of wake type on KC and S is shown in figure 5 for the 20 cases investigated. Test conditions are defined in table 1 for those cases where flow details are presented. As expected, the asymmetric wake forms occur for relatively large values of KC and small values of the stability parameter S, with the suppression of vortex shedding for $S > 0.1$. Considering tests for $KC \approx 9$ we can see that the wake becomes more symmetric as S is increased, changing from a vortex-shedding type for $S < 0.15$ to a symmetric-without-pairing type for $S > 0.28$. While we expect KC and S to be the dominant defining parameters from related studies, dimensional analysis shows that the flow also depends on diameter-to-depth ratio and Reynolds number. These secondary influences may explain results for $S \approx 0.16$, where we see a change from a symmetric-without-pairing wake for $KC < 5$ to a vortex-shedding wake for $KC \approx 8$ and then to a sinuous-with-pairing wake for $KC > 15$. One would expect the degree of asymmetry to increase as KC increases. Over this range of the

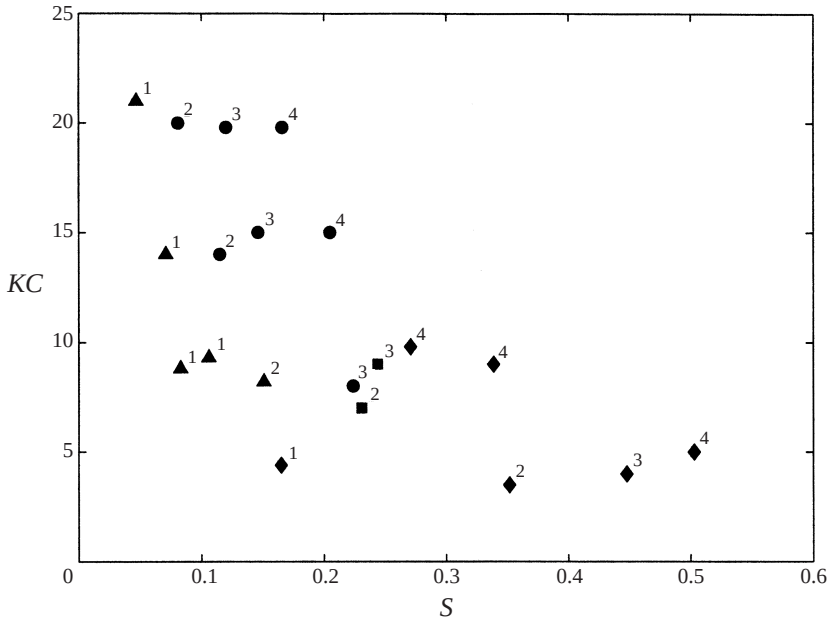

FIGURE 5. Wake classifications for the circular cylinder tests: ▲, vortex shedding; ●, sinuous with pairing; ■, symmetric with pairing; ◆, symmetric without pairing. The superscript associated with each symbol denotes the value of D/h: 1, 10.0; 2, 17.6; 3, 24.0; 4, 33.3.

Name	T (s)	U_o ($\mathrm{m\,s^{-1}}$)	h (m)	D (m)	KC	β	a (m)	Re_a ($\times 10^4$)	c_f ($\times 10^{-3}$)	S	Fr
CC01	75	0.035	0.060	0.60	4.4	4800	0.418	1.46	16.539	0.165	0.046
CC03	140	0.040	0.060	0.60	9.3	2571	0.891	3.57	10.592	0.106	0.052
CC04	140	0.060	0.060	0.60	14.0	2571	1.336	8.02	7.063	0.071	0.078
CC05	140	0.090	0.060	0.60	21.0	2571	2.005	18.05	4.708	0.047	0.117
CC08	120	0.035	0.034	0.60	7.0	3000	0.668	2.34	13.080	0.231	0.061
CC09	120	0.070	0.034	0.60	14.0	3000	1.337	9.36	6.538	0.115	0.121
CC10	120	0.100	0.034	0.60	20.0	3000	1.910	19.10	4.576	0.081	0.173
CC13	120	0.045	0.025	0.60	9.0	3000	0.859	3.87	10.170	0.244	0.091

TABLE 1. Test conditions for the circular cylinder experiments.

stability parameter the diameter-to-depth ratio changes by a factor of 3 and the Stokes parameter β changes by more than 50%.

From figure 5 we see that for $KC < 6$ the wake patterns are in the category of symmetric without pairing. For high values of S however this type of wake can occur with $KC > 6$. An example is shown in figure 6 where digitized dye images (on the left-hand side) and overlaid velocity and vorticity fields (on the right-hand side), produced using the PTV technique, are shown at four times through a half-cycle. The dye visualizations were filmed using a wide-angle lens providing a larger area of view than for the PTV measurements. The vertical component of surface vorticity ($\omega = \partial v/\partial x - \partial u/\partial y$, where u and v are velocities in the x- and y-directions) was calculated from the surface velocity vector field (interpolated on to a regular grid as shown in the figure) by a finite difference approximation. The interpolation procedure used to place velocity vectors on a regular grid may produce poor estimates of velocity

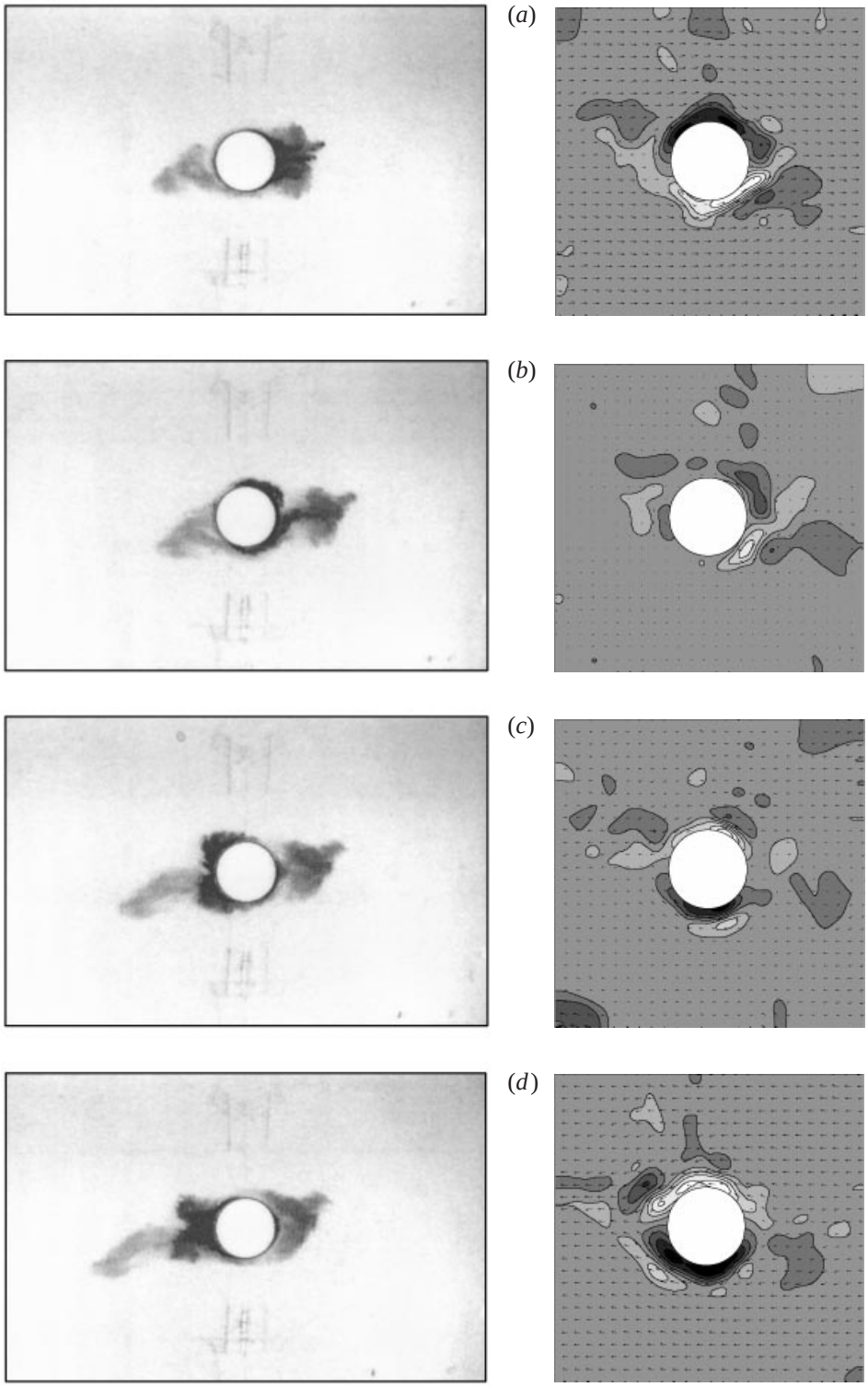

FIGURE 6. Symmetric-without-pairing wake at four times during a tidal period visualized using digitized images of dye visualization tests and velocity and vorticity fields obtained using PTV. Case CC01, $KC = 4.4$, $S = 0.165$. (*a*) $t = T/4$, (*b*) $t = T/2$, (*c*) $t = 5T/8$, (*d*) $t = 3T/4$.

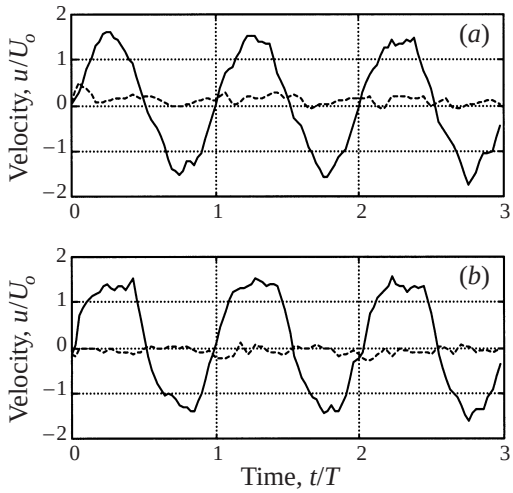

FIGURE 7. Velocity time history for the symmetric-without-pairing case CC01 ($KC = 4.4$, $S = 0.165$) where the velocity is normalized with the free-stream velocity amplitude U_o and time is normalized with the tidal period, T; ——, u-velocity; - - - -, v-velocity. (*a*) $x = 0$ m, $y = 0.45$ m ($= 0.75D$); (*b*) $x = 0$ m, $y = -0.45$ m ($= -0.75D$).

at the extreme edges of the flow domain where extrapolation is necessary to grid that area. In such cases, see for example the top right and bottom left corners of figure 6(*c*), spurious blobs of vorticity may be calculated which should be ignored. The case in figure 6 is CC01 in table 1 with $KC = 4.4$ and $S = 0.165$. In figure 6(*a*) the flow is moving from left to right at the time of the maximum ambient velocity, $t = T/4$. A pair of attached counter-rotating vortices has formed in the near wake which can be seen clearly in the vorticity plot. During flow reversal these vortices convect back past the cylinder almost symmetrically (figure 6(*b*) at $t = T/2$) and decay as a new pair of attached vortices is formed (figure 6(*c*) at $t = 5T/8$). These new vortices remain attached to the cylinder and vortices from the previous half-cycle almost disappear (figure 6(*d*) at $t = 3T/4$). The process continues during the next half-cycle in a repetitive manner. This is similar to the unbounded cylinder wakes observed for $KC < 1$ in numerical simulations (Smith & Stansby 1991).

For selected circular cylinder tests velocity time histories have been constructed from the vector plots produced by the PTV analysis to relate to the vortex structures. The PTV analysis was performed 25 times per period for a total of 3 periods enabling velocities at any position in the flow to be sampled. Although such an analysis is not suitable for measuring the high-frequency velocity components of the flow, it has proved adequate for measuring the low-frequency components produced by the movement of the large-scale vortices outside the main wake regions (Lloyd *et al.* 1995). Velocity time histories measured at opposite sides of the cylinder are shown in figure 7 for the symmetric-without-pairing case discussed above. Figure 7(*a*) shows the velocity at $x = 0$, $y = 0.75D$ (in the top half looking at figure 6) and figure 7(*b*) shows the velocity at $x = 0$, $y = -0.75D$ (in the lower half). At both positions the velocity traces show little or no evidence of the passage of the very weak vortices convecting past the sides of the cylinder during flow reversal and velocities on either side of the cylinder are in phase.

A symmetric-with-pairing wake is shown in figure 8 for case CC08 with $KC = 7.0$ and $S = 0.231$. During flow reversal the attached counter-rotating vortices convect

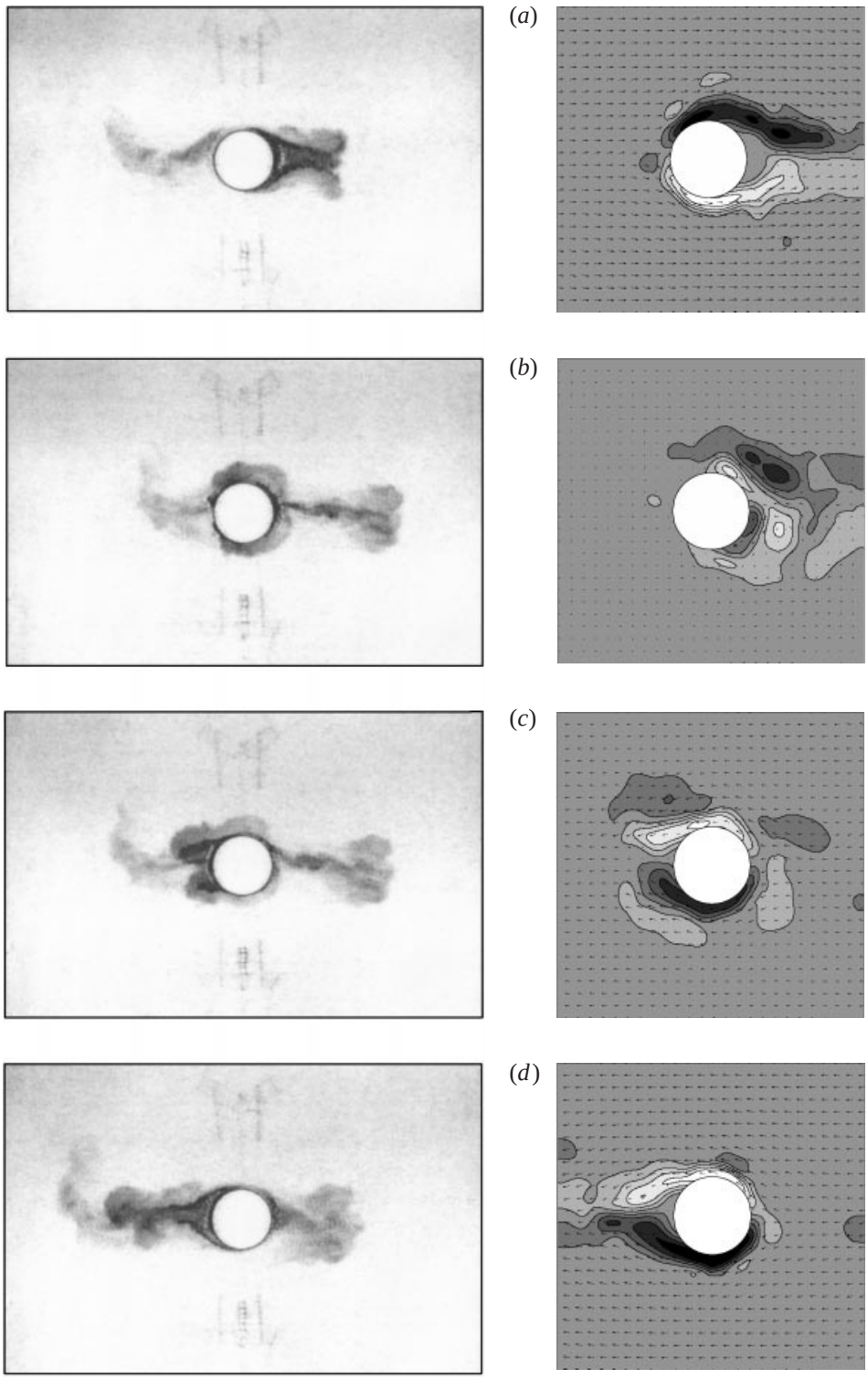

FIGURE 8. Symmetric-with-pairing wake at four times during a tidal period visualized using digitized images of dye visualization tests and velocity and vorticity fields obtained using PTV. Case CC08, $KC = 7.0$, $S = 0.231$. (*a*) $t = T/4$, (*b*) $t = T/2$, (*c*) $t = 5T/8$, (*d*) $t = 3T/4$.

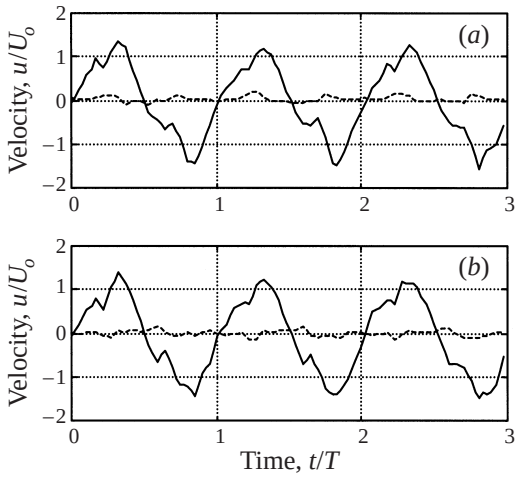

FIGURE 9. Velocity time history for the symmetric-with-pairing case CC08 ($KC = 7.0$, $S = 0.231$) normalized as in figure 7; ——, u-velocity; - - - -, v-velocity. (*a*) $x = 0$ m, $y = 0.45$ m; (*b*) $x = 0$ m, $y = -0.45$ m.

back past the cylinder, forming vortex pairs with vorticity of opposite rotation generated at the sides of the cylinder (figures 8(*b*) and 8(*c*) at $t = T/2$ and $5T/8$). These pairs convect away downstream as 'new' attached counter-rotating vortices are formed (figure 8(*d*) at $t = 3T/4$). For a cylinder in an unbounded flow field with $KC < 4$, Williamson (1985) observed a similar sequence of events. Velocity time histories at opposite sides of the cylinder at the same positions as for the no-pairing case above are shown in figure 9. In contrast to the no-pairing case the movement of the much stronger vortices past the sides of the cylinder during flow reversal show up as double peaks in the u-velocity trace which are approximately in phase on either side of the cylinder.

A sinuous-with-pairing wake is shown in figure 10 for case CC09 in table 1, with $KC = 14.0$ and $S = 0.115$. Figure 10(*a*) shows the wake at $t = T/4$ when the ambient velocity is at its maximum. Two attached counter-rotating vortices have formed in the near wake while the far wake, with its sinuous structure, contains vortex pairs shed during the previous half-cycle; see also figure 10(*b*) at $t = T/2$ when the ambient velocity has reduced to zero. As the flow reverses the near-wake vortices convect back past the cylinder and remain on the same side (of the line through the cylinder centre parallel to the ambient velocity), see figures 10(*b*) and 10(*c*). The asymmetry in the wake is produced by these attached vortices being of different strength and/or size. This is similar to the unbounded cylinder wakes with $4 < KC < 7$ where the vortex pairs were observed to form at different times during flow reversal. This wake asymmetry, and in particular the differing strengths of the oppositely signed vortices, is further illustrated by the velocity time histories shown in figure 11, at the same positions on either side of the cylinder as above. The difference between the time histories is particularly noticeable for the half-period where the ambient flow is from right to left (with negative u-velocity), where the velocity fluctuations associated with the passage of vortices past the bottom half of the cylinder in figure 11(*b*) are approximately twice the magnitude of corresponding fluctuations associated with the vortices sweeping past the top part of the cylinder, shown in figure 11(*a*). Although

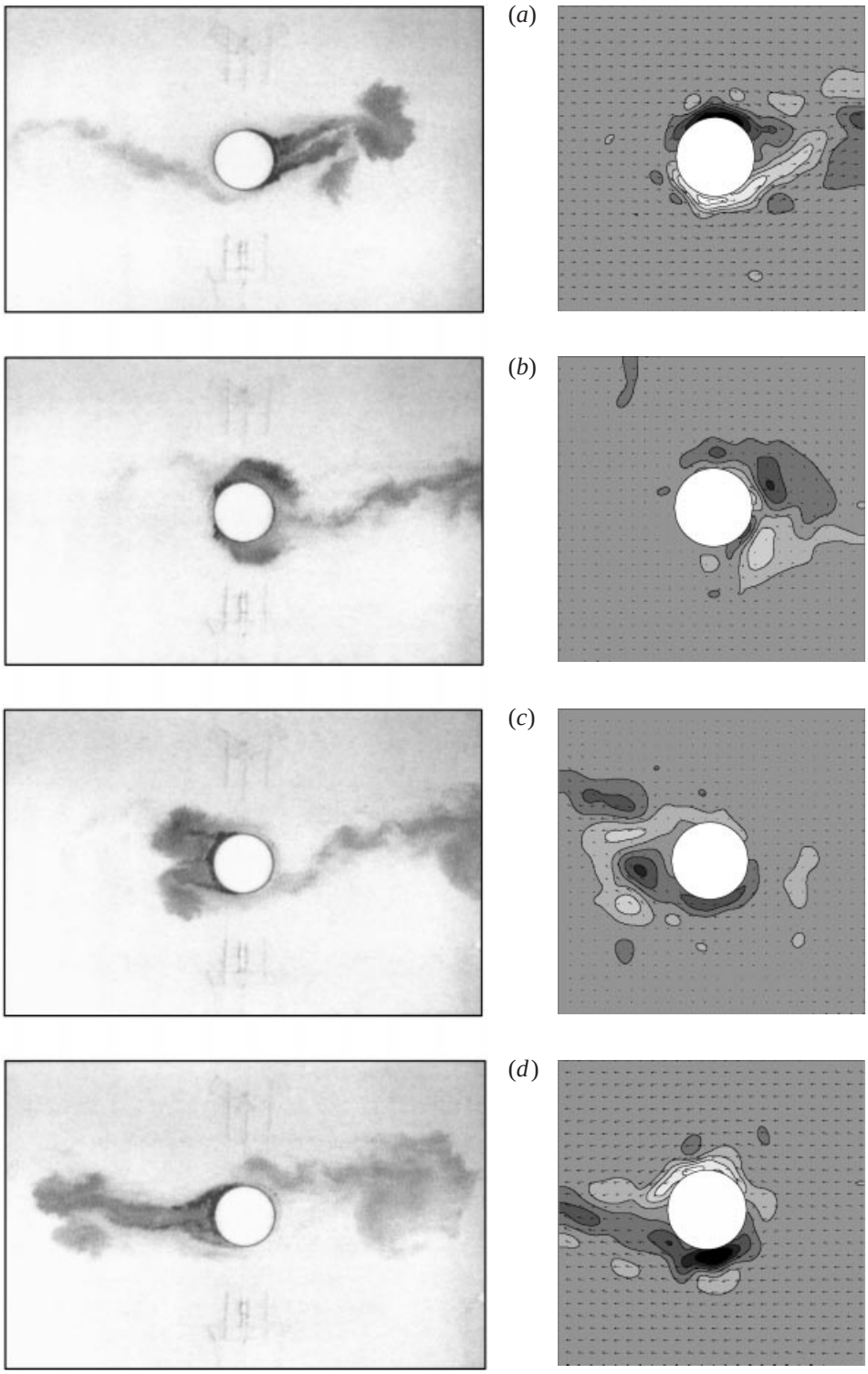

FIGURE 10. Sinuous wake at four times during a tidal period visualized using digitized images of dye visualization tests and velocity and vorticity fields obtained using PTV. Case CC09, $KC = 14.0$, $S = 0.115$. (*a*) $t = T/4$, (*b*) $t = T/2$, (*c*) $t = 5T/8$, (*d*) $t = 3T/4$.

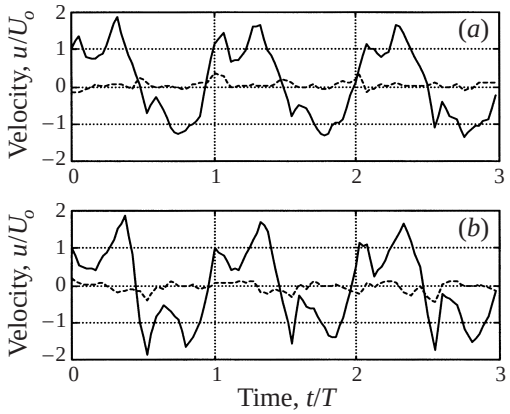

FIGURE 11. Velocity time history for the sinuous case CC09 ($KC = 14.0$, $S = 0.115$) normalized as in figure 7; ——, u-velocity; - - - -, v-velocity. (a) $x = 0$ m, $y = 0.45$ m; (b) $x = 0$ m, $y = -0.45$ m.

the magnitudes of the velocity fluctuations on either side of the cylinder can differ markedly, they remain approximately in phase.

The vortex-shedding wake classification covers a wide range of wake structures, which for an unbounded wake increase in complexity as KC increases, with the number of vortices shed per half-cycle increasing. An example of a vortex-shedding wake is shown in figure 12 for case CC03 with $KC = 9.3$ and $S = 0.106$. To aid interpretation of the dye visualization pictures, arrows have been drawn on the digital images showing the rotation and position of the major vortices. Figure 12(a) shows the wake at $t = T/4$ with two asymmetric, attached, counter-rotating vortices dominating the near field. The anti-clockwise vortex has formed a pair with a clockwise vortex formed during the previous half-cycle and, as the flow decelerates and begins to reverse, we can see that this vortex pair has separated from the cylinder (figure 12(b) at $t = T/2$). The separated anti-clockwise vortex still exerts a strong influence on the near wake causing the attached clockwise vortex to cross to the other side of the cylinder where it then amalgamates with vorticity of the same sign being formed in the next half-cycle (figure 12(c) at $t = 5T/8$). At $t = 3T/4$ in figure 12(d) we see that this region of clockwise vorticity has rolled up to become the dominant vortex in the wake and is on the point of being shed from the cylinder. During the next stage of flow reversal this vortex will shed and the attached vortex on the opposite (upper) side of the cylinder will cross to the lower side. In the following half-cycle both these vortices will convect past the same (lower) side of the cylinder before pairing up to repeat the flow structure shown in figure 12(a). Velocity time histories at the same positions as before are shown in figure 13. The u-velocity trace in figure 13(b) does not show the double peak characteristic of the sinuous and symmetric-with-pairing cases, as the velcoity at that point is dominated by a single large vortex convected back past the cylinder. The peak u-velocity magnitudes in figure 13(b) are greater than in figure 13(a), on the top half of the cylinder, indicating the effect of the vortices convecting back on the lower side of the cylinder. This is also evident in the v-velocity traces, where figure 13(b) shows marked velocity fluctuations and figure 13(a) shows little variation. The prominent difference from the sinuous-with-pairing wake is that an attached near-wake vortex crosses to the other side of the cylinder during flow reversal, while for the sinuous type the attached vortices are convected back on the same sides. However, for both wake types vortex pairing is

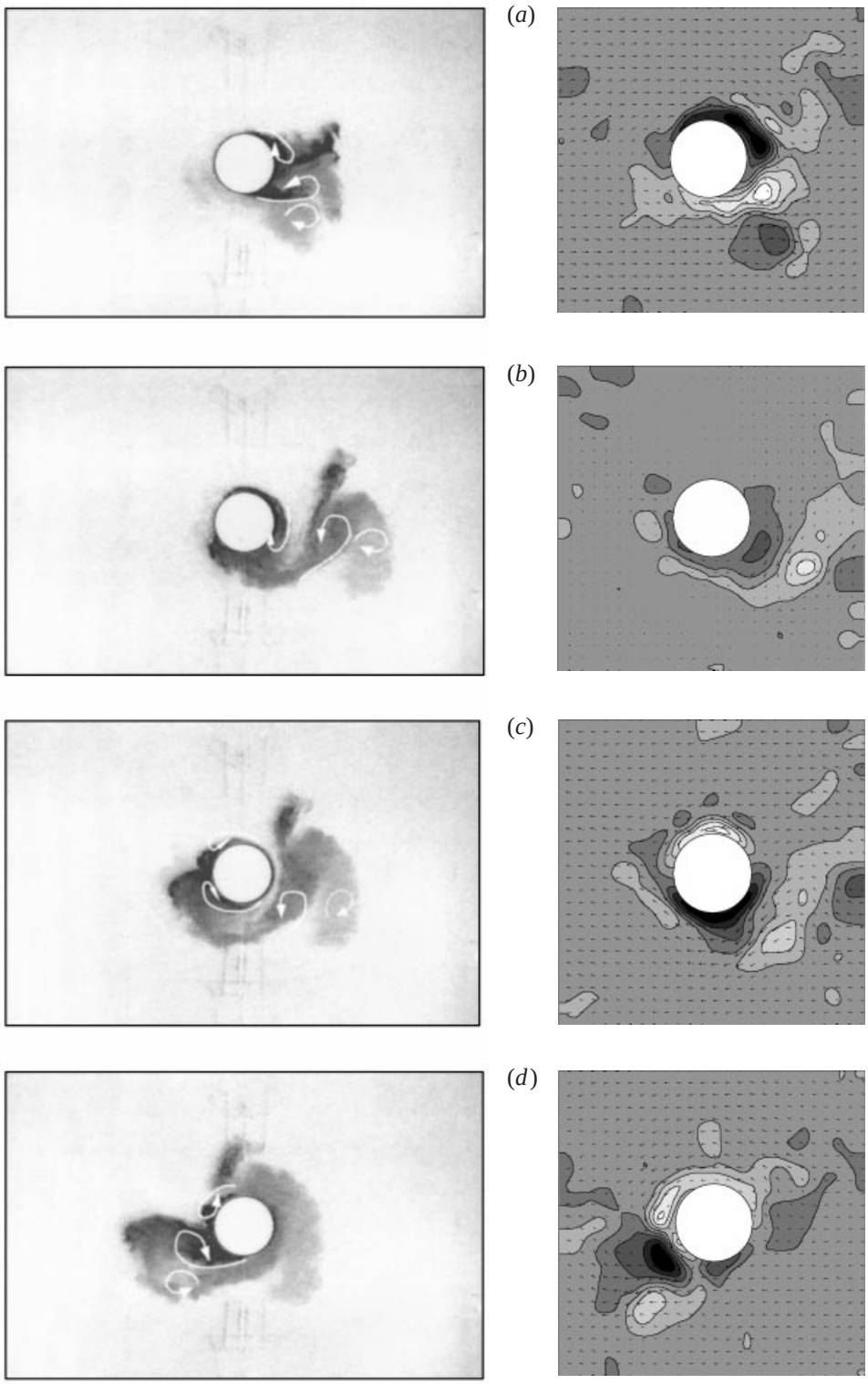

FIGURE 12. Vortex-shedding transverse wake at four times during a tidal period visualized using digitized images of dye visualization tests and velocity and vorticity fields obtained using PTV. Case CC03, $KC = 9.3$, $S = 0.106$. (*a*) $t = T/4$, (*b*) $t = T/2$, (*c*) $t = 5T/8$, (*d*) $t = 3T/4$.

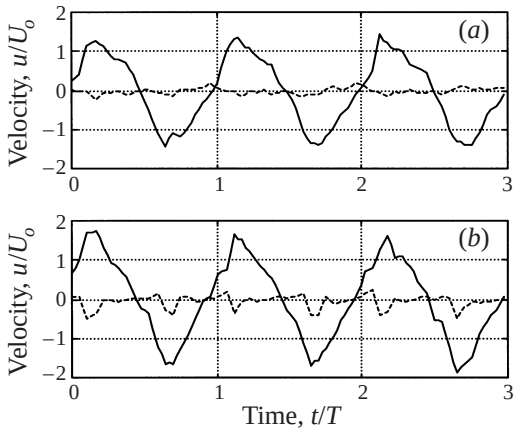

FIGURE 13. Velocity time history for the vortex shedding case CC03 ($KC = 9.3$, $S = 0.106$) normalized as in figure 7; ——, u-velocity; - - - -, v-velocity. (*a*) $x = 0$ m, $y = 0.45$ m; (*b*) $x = 0$ m, $y = -0.45$ m.

an important feature. Williamson (1985) describes a very similar sequence of events for unbounded cylinder wakes with $7 < KC < 13$. In Williamson's experiments, as here, the wake is characterized by the shedding of one dominant vortex per half-cycle with vortex pairing of shed vortices occurring on one side of the cylinder only. Bearman *et al.* (1981) provide sketches of the same type of vortex patterns, calling the range $8 < KC < 15$ the transverse vortex-shedding regime. Williamson calls this a 'transverse street', as vortices convect away from the cylinder to form a street on one side of the cylinder, roughly perpendicular to the oscillation direction. A street of vortices was not observed in the experiments described here, probably owing to the dissipation of vortex energy by bed friction and dispersion caused by the non-uniform vertical velocity variation.

For relatively small values of the stability parameter ($S < 0.1$) the type of wake observed in figure 12 occurred over a KC range similar to that for the transverse street regime in unbounded flow. Figure 14 shows the vortex shedding wake of case CC04 with $KC = 14.0$ and $S = 0.071$. In figure 14(*a*) at $t = T/4$ we see a wake pattern similar to that of the previous case in figure 12(*a*). The near field is dominated by two counter-rotating vortices of different size and strength. The larger clockwise vortex is about to shed and pair up with a vortex of opposite sign from the previous half-cycle. Although it is not clear from the dye visualization images (produced during the first cycle following the release of dye into the flow), this vortex pairing event is apparent in the vorticity plot of figure 14(*a*) and the vortex from the previous half-cycle is sketched on the dye visualization image. Following this, the sequence of events is similar to the previous case although in figure 14 shedding occurs on the upper side of the cylinder. The clockwise vortex is shed (see figure 14*b*) and although the incident flow amplitude is larger than in the previous case it remains close enough to the cylinder to cause the attached anti-clockwise vortex to cross to the opposite (upper) side of the cylinder. This anti-clockwise vorticity amalgamates with the newly generated vorticity on the upper side of the cylinder as the flow reverses (figure 14*c*) to form a vortex pair with the clockwise vorticity from the previous half-cycle (figure 14*d*), as the process is repeated. It is interesting to note that within the narrow range $13 < KC < 15$ Williamson (1985) identified the development of a wake structure not observed in this study. In the so-called 'single-pair' regime the vortex shed during a

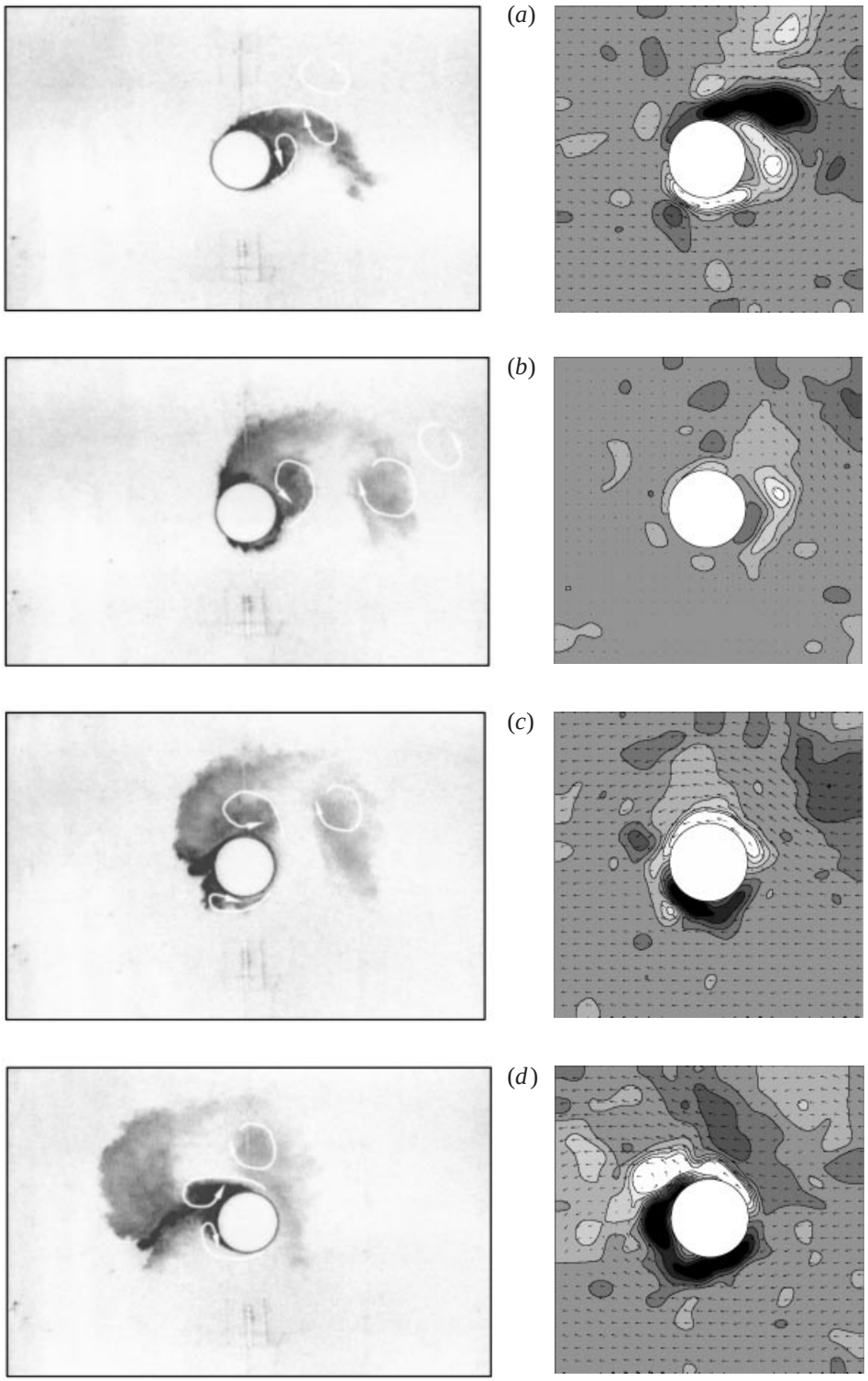

FIGURE 14. Vortex-shedding transverse wake at four times during a tidal period visualized using digitized images of dye visualization tests and velocity and vorticity fields obtained using PTV. Case CC04, $KC = 14.0$, $S = 0.071$. (*a*) $t = T/4$, (*b*) $t = T/2$, (*c*) $t = 5T/8$, (*d*) $t = 3T/4$.

half-cycle (e.g. the clockwise vortex seen in figure 14*a*) convects sufficiently far away from the cylinder so that it no longer dominates the near wake and is unable to induce the attached vortex of opposite sign to cross sides. The end result is a wake which consists of a series of pairs convecting away from the cylinder, on one side only, at around 45° to the incident flow direction.

The single-pair regime is intermediate between the transverse-street wake and the next major vortex-shedding wake type, the 'double-pair' regime identified by both Williamson (1985) and Bearman *et al.* (1981) with $15 < KC < 24$. A double-pair wake is characterized by the shedding of two large vortices in each half-cycle and the formation of two pairs in each cycle. In these shallow-water experiments a double-pair wake was observed with $KC = 21.0$ and $S = 0.047$ (Case CC05) and its development is shown in figure 15. At $t = T/4$ in figure 15(*a*) we can see a pair with an anti-clockwise vortex generated during the previous half-cycle and a clockwise vortex recently shed from the cylinder during the present half-cycle. As the half-cycle progresses this vortex pair will convect downstream away from the cylinder, leaving the near wake dominated by an attached clockwise vortex and a larger shed vortex of anti-clockwise rotation (figure 15(*b*) at $t = T/2$) inducing the attached clockwise vortex to cross to the lower side. In a process similar to that described for the transverse wake, this clockwise vortex then amalgamates with vorticity of the same rotation (figure 15(*c*) at $t = 5T/8$), before pairing up with the anticlockwise vortex from the previous half-cycle and then shedding away from the cylinder. The double-pair wake is notably different from the transverse wake in that, in successive half-cycles, vortex pairs are shed from opposite sides of the cylinder. The attached anti-clockwise vortex shown in figure 15(*d*) will eventually shed from the cylinder, corresponding to the shed anti-clockwise vortex shown in the dye image of figure 15(*b*) in the previous half-cycle.

In unbounded cylinder experiments it has been reported how vortex patterns could repeat for a large number of cycles before changing modes, with separation and shedding changing to the opposite side of the cylinder. Obasaju *et al.* (1988) noted that this change does not occur suddenly, generating a variety of intermediate shedding patterns. The patterns observed in this study were however observed to be broadly repetitive for all cycles recorded (approximately 20).

3.2. *Wake formation for the conical island of* 8° *slope*

Experiments with this geometry in a shallow turbulent steady ambient flow (Lloyd & Stansby 1997) showed that the large-scale features of the wake were similar to those of a vertical circular cylinder investigated by Chen & Jirka (1995). In particular vortex shedding was suppressed if the stability parameter exceeded a critical value of approximately 0.4 (based on the diameter at mid depth for the conical island).

In oscillatory flow the wake structures for the conical island were also found to have a similar classification to those of the cylinder. Figure 16 shows the type of wake observed by the PTV measurements and dye visualization on a (KC, S)-plane. It can be seen that wakes become symmetric as S is increased as for the vertical island case. However, KC is not now a dominant effect. For $S \approx 0.2$ the wakes become more symmetric as KC increases, with D/h also increasing. The underwater shape of the island is of course also changing and simply defining shape by the diameter at mid-depth would appear too simplistic. (Possible Froude number effects will be discussed later.) From figure 16 we see that vortex pairing is suppressed when $S > 0.4$ which compares with $S > 0.25$ for the cylinder case.

Velocity/vorticity plots for the following cases are shown in Part 2 (Stansby &

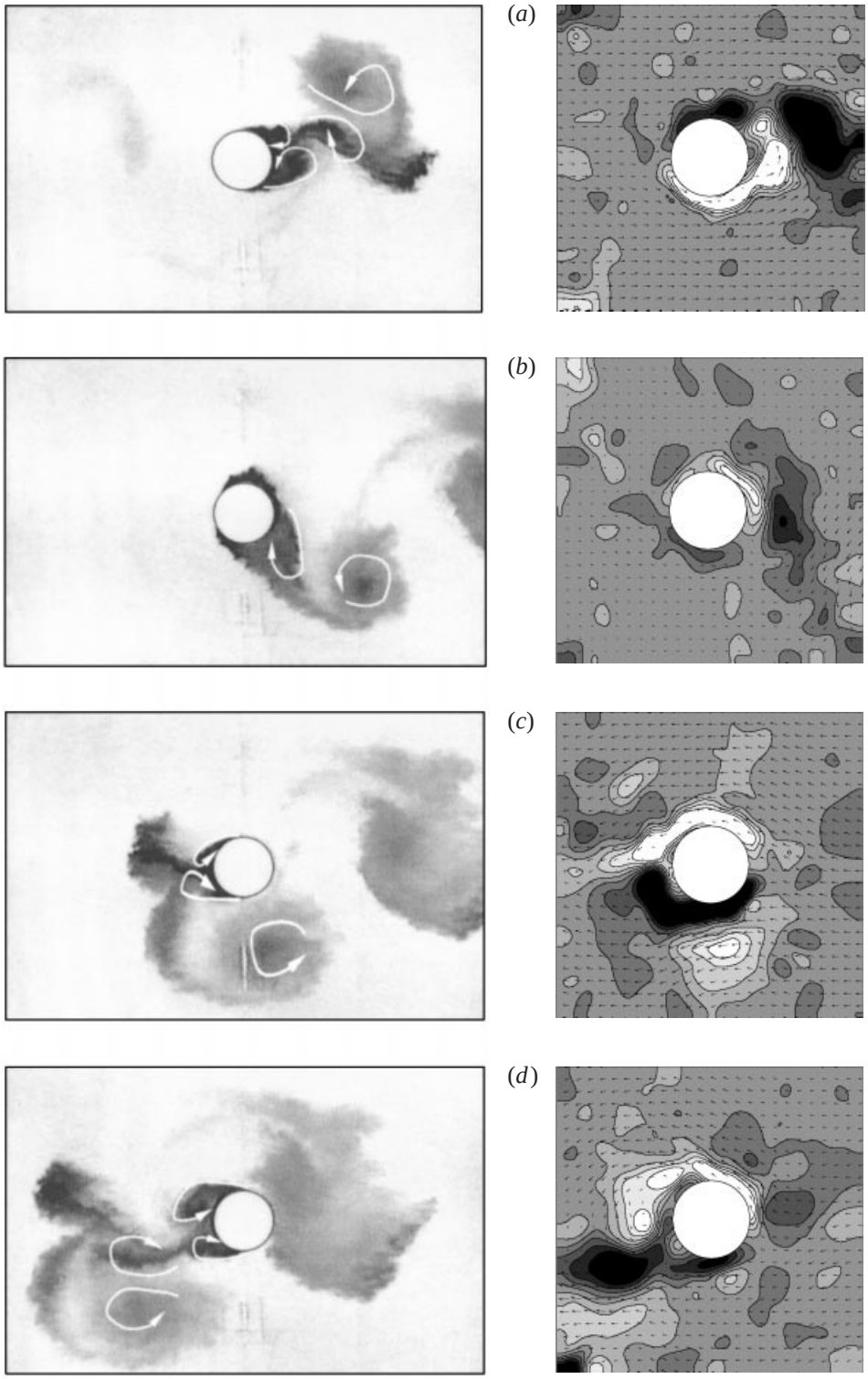

FIGURE 15. Vortex-shedding double pair wake at four times during a tidal period visualized using digitized images of dye visualization tests and velocity and vorticity fields obtained using PTV. Case CC05, $KC = 21.0$, $S = 0.047$. (*a*) $t = T/4$, (*b*) $t = T/2$, (*c*) $t = 5T/8$, (*d*) $t = 3T/4$.

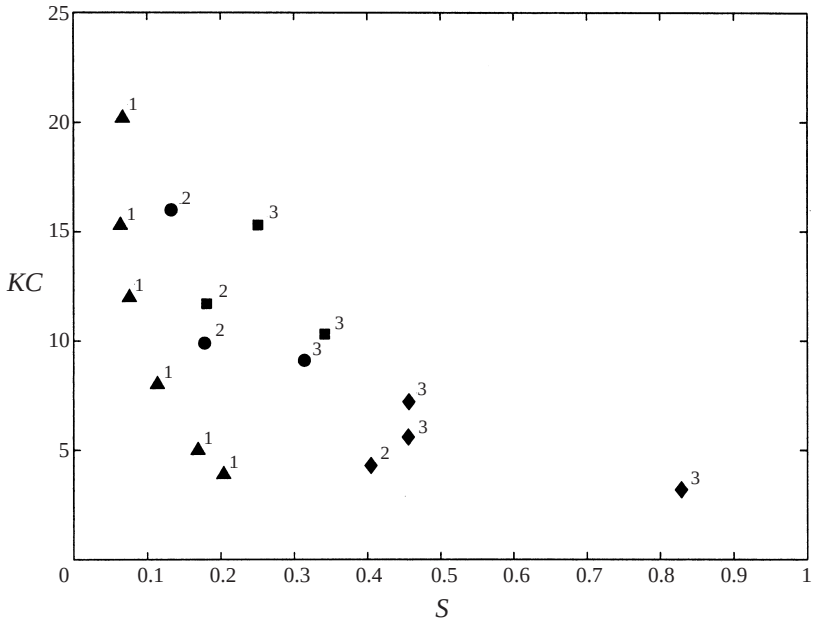

FIGURE 16. Wake classification diagram for the conical island tests: ▲, vortex shedding; ●, sinuous; ■, symmetric with pairing; ◆, symmetric without pairing. The superscript associated with each symbol denotes the value of D/h: 1, 9.15; 2, 21.7; 3, 34.5.

Lloyd 2001) for comparison with numerical modelling: with $KC = 4.3$ and $S = 0.405$ – a symmetric-without-pairing wake similar to the cylinder wake shown in figure 6; with $KC = 15.3$ and $S = 0.251$ – a symmetric-with-pairing wake similar to figure 8; with $KC = 9.9$ and $S = 0.173$ – a sinuous-with-pairing wake similar to figure 10; with $KC = 5.0$ and $S = 0.169$ – a vortex-shedding case similar to figure 12 and to unbounded cylinder wakes within the range $7 < KC < 13$; with $KC = 15.3$ and $S = 0.064$ – a vortex-shedding case similar to figure 15 and to unbounded cylinder wakes with $15 < KC < 24$, showing a double-pair structure.

4. Discussion and conclusions

Experiments conducted in a shallow-water flume with oscillatory flow have identified four distinct types of wake pattern around a circular cylinder or a conical island which are similar to those observed for unbounded cylinder wakes. The results also demonstrate that bed friction can act to stabilize oscillatory wake flows in a similar manner to that found for a steady free stream. The conical island and the cylinder produce wakes with similar large-scale characteristics although the details of the separated flow in the near-wake region will inevitably be quite different.

The four types of wake pattern are: (*i*) symmetric without pairing, (*ii*) symmetric with pairing, (*iii*) sinuous with pairing and (*iv*) vortex shedding. For type (*i*) the wake during each half-cycle is dominated by a pair of counter-rotating eddies attached to the model, similar to the steady-bubble wake generated in a steady flow with a relatively large value of the stability parameter. Type (*ii*) is distinguished from (*i*) by these eddies pairing up with newly formed eddies during flow reversal and convecting away from the cylinder while new attached eddies form. Type (*iii*) is characterized by the vortex pairing losing its symmetry and the wake becomes sinuous. In types (*i*),

(*ii*) and (*iii*) the attached eddies remain on the same sides of the obstacle during flow reversal. In type (*iv*) an attached eddy crosses to the opposite side of the obstacle during flow reversal and vortex shedding occurs. In its simplest form one vortex is shed per half-cycle and the wake structure is quite repetitive. However as KC is increased more vortices can be shed per half-cycle causing more complex wake structures. The wake type is not well defined at a boundary between types, defined here on a (KC, S)-plane, where, for example, vortex shedding and sinuous vortex pairing may interchange.

The wake flows have been defined by the wake stability parameter S, following results for steady current flow, and the Keulegan–Carpenter number KC, following the definition for unbounded wakes. For both the vertical cylinder and conical island cases the wakes generally become more symmetric as S increases. However it is also expected that wakes become more symmetric as KC decreases and, while this is the case for the vertical cylinder, it is not for the island where the effect of D/h and changing underwater geometry appear influential, although the unsteady wake structures are very similar to those which occur with the cylinder. The effect of Froude number has been ignored. For the vertical cylinder flows the maximum ambient Froude number is 0.2 in one case (and less in all others). Local velocities may be higher than the maximum ambient by a factor of less than about 2 (from PTV observation). Froude numbers are thus always less than about 0.4 (and usually much less) and not thought to be significant. For the conical island flows the maximum ambient Froude number is 0.15 (or less) but here the depth tends to zero at the solid/water surface interface. (It is worth repeating that Froude number is based on near-surface velocity and Froude number based on depth-averaged velocity would be somewhat lower.) However wave formation was not noticed in the experiments (other than some small-scale local effects of limited duration) and computational modelling in Part 2 will indicate that Froude number magnitudes are always less than unity.

Since the boundary-layer thickness is less than the water depth over much of the flow domain, shallow-water flow modelling with vertical velocity variation is necessary. (The assumption of a fully developed boundary layer in the depth-averaged formulation would generally underestimate bed friction.) It is of considerable interest to know whether such modelling, with the usual shallow-water assumption of hydrostatic pressure, can reproduce these complex wake formations with their dependence on KC, S and D/h. Applications are restricted to the conical island of small slope. To model the flow around the vertical cylinder would require a full three-dimensional Navier–Stokes solver since boundary layers on the cylinder sides and non-hydrostatic pressure have to be resolved. The three-dimensional hydrostatic pressure shallow-water solver has been developed from that of Stansby (1997).

In these investigations the additional complexity of turbulence has been avoided and, of course, full-scale flows will be turbulent and generally rough turbulent. The main effect of turbulence not accounted for explicitly in the stability parameter is the increase in horizontal diffusion, but it is expected that a broadly similar wake classification in terms of KC, S and D/h will apply but this should be confirmed experimentally.

The support through EPSRC grant no. GR/K76481 is gratefully acknowledged. The experiments were undertaken in the shallow-water flume at the University of Manchester.

REFERENCES

Batchelor, G. K. 1967 *An Introduction to Fluid Dynamics*. Cambridge University Press.

Bearman, P. W., Graham, J. M. R., Naylor, P. & Obasaju, E. D. 1981 The role of vortices in oscillatory flow about bluff cylinders. In *Proc. Intl Symp. on Hydrodynamics in Ocean Engng., Trondheim, Norway, August*, pp. 621–635. Norwegian Hydrodynamic Laboratories, Trondheim, Norway.

Chen, D. & Jirka, G. H. 1995 Experimental study of plane turbulent wakes in a shallow water layer. *Fluid Dyn. Res.* **16**, 11–41.

Chen, D. & Jirka, G. H. 1997 Absolute and convective instabilities of plane turbulent wakes in a shallow water layer. *J. Fluid Mech.* **338**, 157–172.

Chu, V. H., Wu, J.-H. & Khayat, R. E. 1991 Stability of transverse shear flows in shallow open channels. *J. Hydraul. Engng* **117**, 1370–1388.

French, R. H. 1994 *Open-Channel Hydraulics*. McGraw-Hill.

Grubišić, V., Smith, R. B. & Schär, C. 1995 The effect of bottom friction on shallow-water flow past an isolated obstacle. *J. Atmos. Sci.* **52**, 1985–2005.

Hamming, R. W. 1989 *Digital Filters*, 3rd edn. Prentice-Hall.

Ingram, R. G. & Chu, V. H. 1987 Flow around islands in Rupert Bay: An investigation of the bottom friction effect. *J. Geophys. Res.* **92**, 14521–14533.

Jensen, B. L., Sumer, B. M. & Fredsøe, J. 1989 Turbulent oscillatory boundary layers at high Reynolds numbers. *J. Fluid Mech.* **206**, 265–297.

Lloyd, P. M. & Stansby, P. K. 1997 Shallow-water flow around model conical islands of small side slope. Part I: Surface piercing. *J. Hydraul. Engng* **123**, 1057–1067.

Lloyd, P. M., Stansby, P. K. & Ball, D. J. 1995 Unsteady surface velocity field measurement using particle tracking velocimetry. *J. Hydraul. Res.* **33**, 519–534.

Obasaju, E. D., Bearman, P. W. & Graham, J. M. R. 1988 A study of forces, circulation and vortex patterns around a circular cylinder in oscillating flow. *J. Fluid Mech.* **196**, 467–494.

Pattiaratchi, C., James, A. & Collins, M. 1986 Island wakes and headland eddies: A comparison between remotely sensed data and laboratory experiments, *J. Geophys. Res.* **92**, 783–794.

Sarpkaya, T. 1993 Coherent structures in oscillatory boundary layers. *J. Fluid Mech.* **253**, 105–140.

Smith, P. A. & Stansby, P. K. 1991 Viscous oscillatory flows around cylindrical bodies at low Keulegan–Carpenter numbers using the vortex method. *J. Fluids Struct.* **5**, 339–361.

Stansby, P. K. 1997 Semi-implicit finite volume shallow-water flow and solute transport solver with k-ε turbulence model. *Intl J. Numer. Meth. Fluids* **25**, 285–313.

Stansby, P. K. & Lloyd, P. M. 2001 Wave formation around islands in oscillatory laminar shallow-water flows. Part 2. Three-dimensional boundary-layer modelling. *J. Fluid Mech.* **429**, 239–254.

Williamson, C. H. K. 1985 Sinusoidal flow relative to circular cylinders. *J. Fluid Mech.* **155**, 141–174.

Wolanski, E., Imberger, J. & Heron, M. L. 1984 Island wakes in shallow coastal waters. *J. Geophys. Res.* **89**, 10553–10569.